WWW.IJRPR.COM

International Journal of Research Publication and Reviews

Journal homepage: www.ijrpr.com ISSN 2582-7421

Laser Assist Scattering with Muonic Hydrogen Like Atom

Kant Prasad Thapa [a], Saddam Husain Dhobi [b,c*], Kamal Shrestha [a], Topendra Budha [a], Lalmani Acharya [a], Subarna Budhathoki [b], Kishori Yadav [a,c], Suresh Prasad Gupta [a,c]

[a] Department of Physics, Patan Multiple Campus, Tribhuvan University, Patandhoka, Lalitpur, Nepal
[b] Central Department of Physics, Tribhuvan University, Kirtipur, Kathmandu, Nepal
[c] Innovative Ghar Nepal, Lalitpur, Nepal
DOI: https://doi.org/10.55248/gengpi.4.1123.113126

A B S T R A C T

This study delves into the influence of muon positioning on particle behavior within atoms, exploring scenarios where the muon resides inside, outside, or partially inside the nucleus of a hydrogen atom. The observed behavior of the differential cross section (DCS) in these contexts yields significant insights into atomic interactions. When the muon is within the nucleus, a marked decrease in the DCS is noted as the electron's momentum undergoes changes. This suggests a substantial impact of the muon on scattering behavior, akin to phenomena in laser-assisted electron-hole scattering and classical scattering. Conversely, when the muon is outside the nucleus, a sharp decrease in DCS is observed at low momentum changes, in contrast to the behavior observed when the muon is within the nucleus. In cases where the muon is partially internal, an intermediary pattern emerges: exponential decay at lower energies and a gradual decline beyond 1.5 MeV. This behavior bridges the scenarios depicted with the muon inside and outside the nucleus. The findings underscore the pivotal role of muon placement in shaping scattering dynamics within atoms. This enhanced understanding of atomic interactions carries profound implications for the advancement of nuclear physics and our comprehension of the fundamental constituents of matter. The development and computational analysis of corresponding equations were facilitated through the MATLAB student package, bolstering the robustness of the study's conclusions.

Keywords: Muon, Differential cross section, atomic interaction, scattering, muon positioning, Hydrogen atom

Introduction

Muonic atoms represent a unique class of atoms in which a negatively charged muon (μ−) becomes ensnared by an atomic nucleus, establishing a system akin to hydrogen. To facilitate this capture event, muons must be decelerated to a few electron volts (eV), at which point they are subsequently trapped in a high Rydberg state (characterized by a main quantum number n ⩾ 14). Following this initial state, they undergo a cascade process, ultimately transitioning down to the 1s state through a series of collisions, Auger, and radiative transitions. This final step culminates in the emission of muonic x-rays. It's noteworthy that the specific dynamics of this capture and cascade process hinge on factors such as the composition and density of the target material (Stanislaus et al., 1987). Nevertheless, this entire sequence transpires in a matter of a few nanoseconds for low-Z materials (and even more rapidly for higher-Z elements). This timeframe is notably shorter than the temporal resolution of a conventional x-ray detector. Once a muonic atom forms, the muon is highly improbable to transition to another atom, except in the case of muonic hydrogen, which constitutes a neutral system and thus can readily permeate the electron cloud of neighboring atoms (Markushin, 1999). The examination of positive muon μ+-He scattering is pivotal in precision experiments that involve positive muons. This study employs the confined variational technique to explore S-wave μ+-He scattering with scattering momenta below 0.1a−10, where a0 represents the Bohr radius. The adopted method provides precise determinations of S-wave phase shifts and scattering lengths. Applying a modified effective range formula, we ascertain the S-wave scattering lengths to be -12.3a0 for μ+−4He scattering and -10.6a0 for μ+−3He scattering. Additionally, we investigate the distortions induced by μ+ on helium (Wu et al., 2023).

The CREMA collaboration is currently engaged in a high-precision measurement of the ground-state hyperfine splitting (HFS) in muonic hydrogen (μp), aiming for an accuracy of 1 part per million (ppm) through pulsed laser spectroscopy. In this proposed experiment, a laser pulse is employed to excite the μp atom from the singlet to the triplet hyperfine sub-levels. Subsequently, it is returned to the singlet state through an inelastic collision with an H2 molecule. This cycle results in augmented kinetic energy, consequently altering the diffusion pattern of the μp atom within the hydrogen gas and its arrival time at the target walls. This laser-induced adjustment in arrival times is utilized to elucidate the atomic transition. This paper details the simulation of μp diffusion within H2 gas, a crucial component of the experimental design. These simulations have been executed within the Geant4 framework, incorporating various low-energy processes, including the movement of H2 molecules, which accounts for effects linked to the hydrogen target's temperature. The simulations have played a pivotal role in optimizing the hydrogen target parameters (pressure, temperatures, and thickness) and in estimating both signal and background rates. These rates provide essential insights into determining the maximum time required to identify the resonance and the statistical precision achievable in the spectroscopy experiment (Nuber et al., 2023). The calculations of differential cross sections for processes

eqs.(1) (a-d) rely on established scattering amplitudes for μp interacting with single protons. These computations also consider factors like the molecular binding of protons in H2, electron screening, and spin correlations for specific rotational states of H2. A method for computing partial differential cross sections is detailed in references, with numerical results available for energies up to 100 eV. The total cross sections σ CM if, as depicted in Fig. 2, vary with collision energy in the center of mass (CM) frame of the μp + H2 system. Here, i and f represent the total spin of the initial and final hyperfine states, respectively. It's worth noting that these cross-sections encompass all conceivable ro-vibrational excitations of the H2 molecule. Calculations of the differential cross sections for the processes in Eqs. (1)(a-d) use the cross sections for the corresponding "nuclear" scattering processes of μp on single protons, for which scattering amplitudes are available (Bubak and Faifman, 1987). In addition, they take into account effects of molecular binding of the protons in H2, electron screening and spin correlations for specific rotational states of H2 . A method for calculating the partial differential cross sections of these processes is described (Adamczak, 2006) and the numerical results for the cross sections are tabulated for energies ⩽ 100 eV. The total cross sections σ CM are given in Fig. 2 as a function of collision energy in the CM frame of the μp + H2 system.

Muonic atom spectroscopy, a technique for studying x-ray emissions during muonic atom formation, has been instrumental in investigating nuclear shape and size. This method has been applied to nearly all stable elements, yielding highly accurate absolute charge radii. However, previous experiments required large targets of several hundred milligrams to stop a muon beam and form the muonic atom. A new approach has been developed, utilizing repeated transfer reactions within a high-pressure hydrogen gas cell with a small amount of deuterium. This innovation significantly reduces the required target material while maintaining satisfactory efficiency. Detailed simulations of the transfer reactions align with experimental data, indicating a solid grasp of the processes within the gas mixture. To validate this method, a measurement of the 2p-1s muonic x rays from a 5 μg gold target is presented as a proof of principle (Adamczak et al., 2023). The research presented highlights various aspects of muonic atoms, including their formation and behavior in different environments. However, a noticeable research gap exists in the investigation of Laser Assisted Scattering with Muonic Hydrogen-like Atoms. This area remains unexplored in the referenced literature. This gap suggests a potential avenue for future studies to delve into the interactions and properties of muonic hydrogen-like atoms under the influence of laser assistance. Such research could provide valuable insights into the behavior of these exotic atoms in novel experimental conditions. The significance of the article lies in its exploration of a novel and previously unexplored aspect of muonic atoms. While the provided information covers various aspects of muonic atom behavior, it notably lacks investigation into the interactions and properties of muonic hydrogen-like atoms under the influence of laser assistance. This represents a crucial research gap. The article thus introduces a pioneering approach that employs laser assistance in the study of muonic hydrogen-like atoms. By doing so, it contributes to expanding our understanding of the behavior and characteristics of these exotic atoms under unique experimental conditions. This research could have significant implications for both theoretical and applied physics, potentially leading to advancements in various scientific and technological fields.

Nomenclature

DCS: DCS: differential cross section

CM: center of mass

e-H: Electron Hydrogen

MeV: Mega electron volt

μp: muonic hydrogen

Materials and Methods

Materials and Methods

Muonic atoms are employed to investigate nuclear properties due to the close proximity of bound or captured muons to the nucleus, providing highly precise information about nucleons. This study focuses on two nuclear properties determined by measuring the X-ray spectrum: absolute nuclear charge radius and the quadrupole moment of the nucleus. Since muon capture occurs at the nucleus, we categorize the capture region into three types: muons entirely captured within the nucleus, muons bound to the nucleus outside it, and muons partially captured and bound by the nucleus. The muon capture regions are further classified into three zones: $\boldsymbol{r \leq R_N - R_\mu}$ (muon completely inside the nucleus), $\boldsymbol{R_N - R_\mu < R_N + R_\mu}$ (muon partially inside the nucleus), and $\boldsymbol{r > R_\mu - R_N}$ (muon completely outside the nucleus). Here, R_N represents the nucleus radius, R_μ signifies the radius of muonic charge, and r denotes the distance between the nuclear and muonic charge centers. The interaction potential is assumed to follow a general form (Khan, 1973 and Sen, 1963).

$$\boldsymbol{V(r) = -Ze^2 f_i(r), i = 1,2,3} \quad (\mathbf{1})$$

When muon is inside the nucleus $(r < R_N - R_\mu)$ then from equation (1) we have

$$\boldsymbol{V(r) = -\frac{Ze^2}{R_N}\left(\frac{3}{2} - \frac{3}{10}R_\mu^2 R_N^{-2} - \frac{1}{2}r^2 R_N^{-2}\right)} \quad (\mathbf{2})$$

When muon is completely outside the nucleus $(r \geq R_N + R_\mu)$ then from equation (1) we have

$$\boldsymbol{V(r) = -\frac{Ze^2}{r}} \quad (\mathbf{3})$$

When muon is partially inside the nucleus $(R_N - R_\mu < r < R_N + R_\mu)$ then from equation (1) we have

$$V(r) = -Ze^2\left(\frac{d_{-1}}{r} + d_0 + d_1 r + d_2 r^2 + d_3 r^3 + d_5 r^5\right) \quad (4)$$

Where $d_{-1} = \frac{1}{2} + \frac{1}{32}\left(R_\mu R_N^{-1} + R_\mu^{-1} R_N\right)\left(R_\mu^2 R_N^{-2} - 10 + R_\mu^{-2} R_N^2\right)$, $d_0 = \frac{3}{4}\left\{R_N^{-1}\left(1 - \frac{R_\mu^2 R_N^{-2}}{5}\right) + R_\mu^{-1}\left(1 - \frac{R_\mu^{-2} R_N^2}{5}\right)\right\}$, $d_1 = \frac{9}{32}\left(R_N^{\frac{1}{2}} R_\mu^{-\frac{3}{2}} - R_\mu^{\frac{1}{2}} R_N^{-\frac{3}{2}}\right)$,

$d_2 = -\frac{1}{4}\left(R_N^{-3} + R_\mu^{-3}\right)$, $d_3 = \frac{3}{32}\left(R_N^{-2} + R_\mu^{-2}\right)\left(R_N R_\mu\right)^{-1}$, $d_5 = -\frac{\left(R_N R_\mu\right)^{-3}}{160}$.

The Schrodinger time-dependent equation's wave function (Bransden and Joachain, 2003) is

$$X(r,t) = 1\frac{1}{(2\pi)^{3/2}}\, exp\{i\frac{p}{\hbar}\cdot(r + \frac{e}{m}\int A(t')dt' - i\frac{E}{\hbar}t - i\frac{e^2}{2m\hbar}\int A^2(t')dt' \quad (5)$$

Equation (5) is Volkov wave function, E is the free electron's kinetic energy. Keep in mind that the momentum operator's eigenvalue is $\hat{p}$. The Volkov wave function's general form is given by equation (5) is obtained with vector potential as shown in equation (6)

$$X(r,t) = \frac{1}{(2\pi)^{\frac{3}{2}}}\, exp\left\{-\frac{i}{\hbar}\left(E + \frac{e^2a^2}{4m}\right)t + i\frac{p}{\hbar}\cdot\left(r\frac{e\,a}{m\omega}\, sin(\omega t)\right) - i\frac{e^2a^2}{8m\hbar\omega}\, sin(2\omega t)\right\} \quad (6)$$

This equation explains the wave function of electrons in a laser field.

$$S_{fi} = \delta_{fi} - \frac{i}{\hbar}\int_{-\infty}^{+\infty}\langle X_f(r,t)|V(r)|\Psi_i(r,t)\rangle dt' \quad (7)$$

Using the first-Born approximation, let's calculate the time integral by supposing that the scattered potential is low.

$$\int_{-\infty}^{+\infty}\langle X_f(r,t)|V(r)|X_i(r,t)\rangle dt' = \frac{1}{(2\pi)^3}\frac{i}{\hbar}\int_{-\infty}^{+\infty} e^{i(E_f - E_i)t'/\hbar}dt' \times \int_{-\infty}^{+\infty} exp\{-i\frac{e}{m\hbar\omega}Q\cdot a\, sin(\omega t)\}dt' \times \int V(r)e^{-i(Q\cdot r)/\hbar}d^3r' \quad (8)$$

When the momentum transfer formula $q = p_f - p_i$ was utilized. On using equation (2) in equation (8) and considering r is very large: In this case, if r is very large, e^{iqr}/e^{-iqr} oscillates rapidly between $e^{iqr}/e^{-iqr} \approx -1$ and $e^{iqr}/e^{-iqr} \approx 1$, because the unit circle is being traversed many times. If r is very, very large, these oscillations will be so rapid that the average value of e^{iqr}/e^{-iqr} over any finite interval will tend towards zero. So, in this case, you can often neglect e^{iqr}/e^{-iqr} compared to $(1-iqr)/(1+iqr)$ if the magnitude of $(1-iqr)/(1+iqr)$ is significant. When r is very small: In this case, if r is very small, e^{iqr}/e^{-iqr} will be close to 1 because the exponential function e^{iqr}/e^{-iqr} approaches 1 as r approaches 0. So, if r is very small, e^{iqr}/e^{-iqr} can often be approximated as 1

and neglected compared to $(1-iqr)/(1+iqr)$ if the magnitude of $(1-iqr)/(1+iqr)$ is significant. The Scattering amplitude of the first born approximation inside is calculated as

$$f_{Born}^{I} = \frac{4\pi\hbar}{q}\left(-\frac{rR_\mu^2}{5qR_N^2} - \frac{3r}{q} + \frac{(2q^2r^3 - 12r)}{q^3R_N^2}\right) \quad (9)$$

Similarly for (8) and (3) scattering amplitude of the born approximation outside is calculated as

$$f_{Born}^{O} = -\frac{2\hbar}{q^2} \quad (10)$$

Similarly from (4) and (8) the scattering amplitude of the born approximation for partially inside is calculated as

$$f_{Born}^{P} = \frac{Zme^2}{2q\hbar}\left(-2\frac{d_{-1}}{q} - 2qr\frac{d_0}{q^2} + \frac{d_1(-2q^2r^2+4)}{q^3} + \frac{d_2(-2q^3r^3+12qr)}{q^4} + \frac{d_3(-2q^4r^4+24q^2r^2-48)}{q^5} + \frac{d_5(-2q^6r^6+60q^4r^4-720q^2r^2+1440)}{q^7}\right) \quad (11)$$

Now, the S matrix can be expressed from above for the n^{th} element.

$$S_{fi} = \delta_{fi} - i2\pi\delta(E_f - E_i + \mathrm{n}\hbar\omega)\left[-\frac{1}{(2\pi)^3}\frac{2\pi\hbar^2}{m}J_n\left(-\frac{e}{m\hbar\omega}(q.a)\right)f_{Born}\right] \quad (12)$$

Comparing equation (10) with standard scattering matrix equation the recognizing T_{fi} matrix is obtained as,

$$T_{fi} = -\frac{1}{(2\pi)^3}\frac{2\pi\hbar^2}{m}J_n\left\{-\frac{e}{m\hbar\omega}(q.a)\right\}\ f_{Born} \quad (13)$$

Now the DCS is obtained in a.u. term as

$$\frac{d\sigma_{FF}^{n}}{d\Omega} = \frac{k_f}{k_i}\left|J_n\left\{-\frac{e}{m\hbar\omega}(q.a)\right\}f_{Born}\right|^2 \quad (14)$$

Also, for zero order Bessel function, $J_0 = 1$ and hence (12) equation become

$$\left(\frac{d\sigma}{d\Omega}\right)_{J_0} = \frac{k_f}{k_i}|f_{Born}|^2 \quad (15)$$

For Inside the DCS from (9) and (15) is

$$\left(\frac{d\sigma}{d\Omega}\right)_I = \frac{`16\pi k_f}{q^2 k_i}\left|-\frac{rR_\mu^2}{5qR_N^2}-\frac{3r}{q}+\frac{(2q^2r^3-12r)}{q^3R_N^2}\right|^2 \quad (16)$$

For Outside the DCS from (10) and (15) is

$$\left(\frac{d\sigma}{d\Omega}\right)_O = \frac{k_f}{k_i}\left|\frac{2}{q^2}\right|^2 \quad (17)$$

For Partially inside the DCS from (11) and (15) is

$$\left(\frac{d\sigma}{d\Omega}\right)_P = \frac{k_f}{4q^2k_i}\left|-2\frac{d_{-1}}{q}-2qr\frac{d_0}{q^2}+\frac{d_1(-2q^2r^2+4)}{q^3}+\frac{d_2(-2q^3r^3+12qr)}{q^4}+\frac{d_3(-2q^4r^4+24q^2r^2-48)}{q^5}+\frac{d_5(-2q^6r^6+60q^4r^4-720q^2r^2+1440)}{q^7}\right|^2 \quad (18)$$

Results and Discussion

The development of DCS for insider outside and partially inside of muon in nucleus of hydrogen atom are developed in equation (17), (18) and (19). The computed nature of equation is shown in Fig. 1, Fig. 2 and Fig. 3, respectively. For computing the nature online MATLAB student package is used. The nature of DCS with change in energy of momentum of incidence electrons shows decrease, more detail in Fig. 1, Fig. 2 and Fig. 3 for inside, outside and partially inside of muon, respectively

3.1. DCS When Muon is inside the Nucleus of Hydrogen Atom

Fig. 1, illustrate the behavior of the differential cross section (DCS) in response to changes in the momentum of an electron under the influence of a laser field. The key observation in Fig. 1 is that the DCS decreases as the momentum of the electron changes, particularly when a muon is located inside the nucleus. This suggests a noteworthy influence of the muon on the scattering behavior. Furthermore, it is asserted that the observed nature of this phenomenon bears a resemblance to both laser-assisted electron-hole (e-H) scattering and classical scattering. This finding holds significant implications when compared to previous research. Previous studies have primarily focused on elucidating the behavior of DCS in various contexts. However, the incorporation of a muon within the nucleus, as explored in Fig. 1, presents a unique and intriguing addition to the body of knowledge. This introduces a novel factor that significantly alters the scattering dynamics, leading to the observed decrease in DCS with changing electron momentum. The specific interaction between the muon and the electron, within the confines of the nucleus, likely plays a crucial role in this phenomenon. This insight aligns with prior investigations into similar scattering processes, specifically laser-assisted e-H scattering and classical scattering.

The similarity observed with these established phenomena suggests a unifying principle that may underlie a broader class of scattering processes. This convergence of behavior across different systems invites further theoretical exploration and experimental validation. Additionally, the comparison to classical scattering implies that there may be underlying principles governing the interaction, which transcend classical and quantum mechanical descriptions. This presents an exciting avenue for future research, potentially offering a deeper understanding of the fundamental physics at play in these intricate scattering processes.

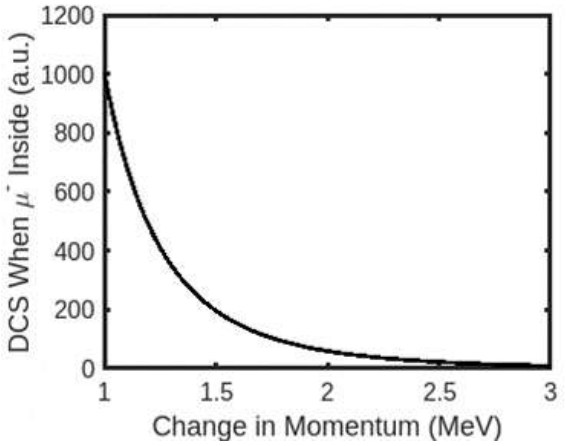

Fig. 1: Change in Momentum vs DCS when muon is inside the nucleus

3.2. DCS When Muon is Outside the Nucleus of Hydrogen Atom

The behavior of DCS in response to changes in the momentum of an electron when a muon is located outside the nucleus, as depicted in Fig. 2. The key observation in Fig. 2 is that the DCS exhibits a sharp decrease when the exchange in momentum of the electron is low. However, in regions characterized by a high exchange of momentum, the DCS remains nearly constant. Notably, this pattern of behavior contrasts with the findings in Fig. 1, where the muon was situated inside the nucleus. This observed behavior in Fig. 2 holds intriguing implications for our understanding of scattering processes. The sharp decrease in DCS at low momentum changes suggests that there is a threshold below which the scattering process is significantly suppressed. This could be attributed to the muon's presence outside the nucleus, which may alter the dynamics of the electron-muon interaction. In this scenario, the electron's behavior is likely influenced by the muon's charge and mass, resulting in a distinctive scattering pattern. Conversely, the constancy of DCS in regions of high momentum exchange is a notable departure from the behavior seen in Fig. 1. This implies that, in the presence of a muon outside the nucleus, the scattering process becomes less sensitive to changes in electron momentum within certain ranges. This could be due to the altered electrostatic potential field around the nucleus, influenced by the muon's position. Comparatively, when the muon is located inside the nucleus, as depicted in Fig. 1, the scattering behavior exhibited a different trend. The decrease in DCS with changing electron momentum, particularly in the presence of the muon, suggests a significant influence of the muon's proximity to the nucleus. This could be attributed to complex interactions involving the electron, muon, and nucleus, which lead to the observed decrease in scattering probability.

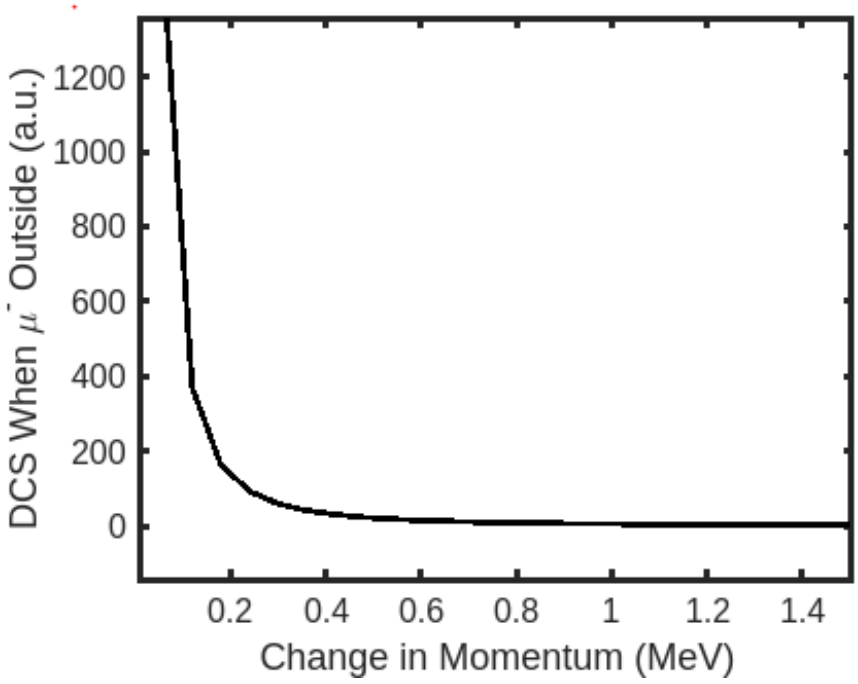

Fig. 2: Change in Momentum vs DCS when muon is outside the nucleus

3.3. DCS When Muon is partially inside the Nucleus of Hydrogen Atom

The behavior of DCS, when muon is inside nucleus is illustrated in Fig. 3. This Fig. demonstrates that the DCS exhibits an exponential decay pattern when the exchange energy of the electron is lower. However, as the exchange energy surpasses 1.5 MeV, the DCS experiences a gradual decrease. This behavior is observed when the muon is partially situated within the nucleus. Importantly, this nature of DCS behavior in Fig. 3 can be considered as a specific case between the findings in Fig. 1 (where the muon is entirely inside the nucleus) and Fig. 2 (where the muon is outside the nucleus). The exponential decay of DCS at lower exchange energies in Fig. 3 suggests a highly sensitive response to changes in the electron's exchange energy. This behavior could be attributed to the intricate interplay between the electron, muon, and the surrounding nuclear environment. At lower exchange energies, the electron's interaction with the muon and the nucleus may lead to a rapid decrease in the probability of scattering events. Conversely, as the exchange energy exceeds 1.5 MeV, the DCS experiences a more gradual decrease. This shift in behavior indicates that at higher exchange energies, the scattering process becomes less influenced by changes in the electron's energy. This could be attributed to the dynamic balance of forces and energies involved in the interaction, leading to a more stable scattering probability. The observation that this behavior occurs when the muon is partially inside the nucleus is particularly significant. It implies that the muon's positioning, even partially, has a discernible impact on the scattering dynamics. The muon's presence affects the electron's motion and interaction with the nucleus, leading to the specific DCS pattern observed in Fig. 3. Furthermore, the nature of DCS in Fig. 3 can be understood as an intermediate case between Fig. 1 and Fig. 2. In Fig. 1, where the muon is entirely inside the nucleus, a significant decrease in DCS is observed, indicating a strong influence of the muon's presence. In Fig. 2, where the muon is outside the nucleus, the DCS exhibits different characteristics, suggesting altered scattering dynamics. Fig. 3, with the muon partially inside the nucleus, bridges these two scenarios, providing a nuanced understanding of how the muon's position impacts the scattering process.

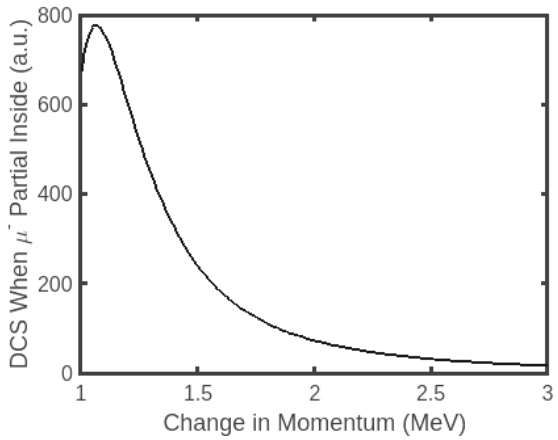

Fig. 3: Change in Momentum vs DCS when muon is partially inside the nucleus

Conclusion

The influence of muon positioning on particle behavior within atoms was study in this work. When the muon was inside the nucleus, observation shows a significant change in the scattering pattern as the exchange momentum varied. Conversely, with the muon outside, a different trend emerged. In cases where the muon was partially inside the nucleus, an intermediate pattern was noted: rapid decrease at lower speeds, and stability at higher speeds. This underscores the critical role of muon placement in scattering dynamics. These findings deepen our understanding of atomic interactions, offering pivotal insights for further advancements in nuclear physics and the study of matter's fundamental constituents.

Acknowledgements

The authors express their gratitude to the faculty members at Innovative Ghar Nepal for generously providing research space. Additionally, they would like to extend their appreciation to the faculty at the Department of Physics, Patan Multiple Campus, and the Central Department of Physics, Tribhuvan University, Nepal, for their motivation and insightful discussions pertaining to this study.

REFERENCES

Khan, M. H. (1973). Muonic X-Rays and Equivalent Radius of Nuclear Charge Distribution (Doctoral dissertation, Texas Tech University). Retrieved from http://ttu-ir.tdl.org/bitstream/handle/2346/13345/31295015065534.pdf?sequence=1

Sens, J. C. (1963). Muon and Nuclear Structure. CERN. http://cds.cern.ch/record/862723/files/vii.pdf

Bransden, B. H., & Joachain, C. J. (2003). Physics of Atoms and Molecules (2nd ed.). Prentice Hall.

Stanislaus, S., Entezami, F., & Measday, D. F. (1987). Atomic capture of muons and density. Nuclear Physics A, 475(4), 642–656. https://doi.org/10.1016/0375-9474(87)90230-2

Markushin, V. E. (1999). Cascade in muonic and pionic atoms with Z = 1. Hyperfine Interactions, 119, 11. https://doi.org/10.1023/A:1012642215730

Wu, M.-S., Zhang, Y., Yan, G.-A., Zhang, J.-Y., Varga, K., & Yan, Z.-C. (2023). Elastic scattering of positive muons from 3He and 4He. Physical Review A, 107, 042815. https://doi.org/10.1103/PhysRevA.107.042815

Nuber, J., Adamczak, A., Abdou Ahmed, M., Affolter, L., Amaro, F. D., Amaro, P., ... Zhang, J. (2023). Diffusion of muonic hydrogen in hydrogen gas and the measurement of the 1s hyperfine splitting of muonic hydrogen. SciPost Physics Core, 6(057).

Adamczak, A. (2006). Differential cross sections for muonic atom scattering from hydrogenic molecules. Physical Review A, 74, 042718. https://doi.org/10.1103/PhysRevA.74.042718

Bubak, M., & Faifman, M. P. (1987). Cross sections for hydrogen muonic atomic processes in two-level approximation of the adiabatic framework (Report No. JINR-E4-87-464).

Adamczak, A., Antognini, A., Berger, N., Cocolios, T. E., Deokar, N., Düllmann, Ch. E., ... Wauters, F. (2023). Muonic atom spectroscopy with microgram target material. The European Physical Journal A, 59(15). https://doi.org/10.1140/epja/s10050-023-00930-y